Effect of Sintering Temperature on the Dielectric Properties of Non-stoichiometric Nickel Oxide

Paras Dubey[1, a)] , K. K. Choudhary[2], Kiran Singh[3,4], and Netram Kaurav[1, a)]

[1]*Department of Physics, Government Holkar Science College,, Indore 452001, India*
[2]*Army Cadet College, Indian Military Academy, Dehradun, (UK) India-248007*
[3]*UGC-DAE Consortium for Scientific Research, University Campus, Khandwa Road Indore-452001, India*
[4]*(Present Address)Department of Physics, Dr. B.R. Ambedkar National Institute of Technology Jalandhar (Punjab) - 144 011 India*

[a)] *Corresponding author: paras_dubey74@yahoo.co.in, netramkaurav@yahoo.co.uk*

Abstract. Non-stoichiometric nickel oxide was synthesized by solid state route method at different sintering temperatures upto 1100 °C. The structure of synthesized compounds were analyzed by X ray diffraction analysis (XRD) and the dielectric constant was found to different for samples of different stoichiometry. These results were interpreted as the decomposition temperature increases, which heals the defects present in the non-stoichiometric nickel oxide and loss peak shifts to the higher frequency which is due to long range hopping of charge carriers.

INTRODUCTION

Nickel oxide (NiO) is the most comprehensively investigated transition metal oxide over the decades [1]. NiO is one of the promising and environment friendly *p-type* semiconductors with wide band gap energy ranging from 3.6 to 4 eV (bulk form). NiO is a very interesting material due to its complex band structure. Stoichiometric NiO (Ni_{50} O_{50}) is a Mott-Hubbard insulator with room temperature conductivity of less than 10^{-13} S cm^{-1}. Very low conductivity of NiO may be due to hopping of charge carriers associated with Ni^{2+} vacancies [2]. NiO has been considered as a promising functional material for varieties of applications, such as, smart windows [3], spin valves giant magneto resistance (GMR) sensor [4], solar cells [5], gas sensors [6], high permittivity dielectric material and electrochromic material for displays [7], photoelectrolysis [8], etc. several efforts have been made to explain the insulating behavior of NiO, were in, appreciable conductivity can be achieved in NiO by creating Ni vacancies or substitution at nickel side, thereby creating Ni vacancies and the composition ratio of Ni and O changes and NiO becomes non-stoichiometric. Hence various property, including dielectric behavior changes in non stiochiometric nickel oxide, this can be attributed to presence of excess oxygen. However, when NiO is anti-ferro magnetically ordered or defect-rich, the dielectric loss increases significantly [9]. In the present work the dielectric property in non stoichiometric NiO, produced by thermal decomposition route, was studied.

EXPERIMENTAL PROCEDURE

Following [10, 11] nickel nitrate hexa-hydrate [$Ni(NO_3)_2.6H_2O$] sintered at different temperature, which was decomposed to produced nickel oxide samples of various stoichiometries[12]. Nickel nitrate hexa-hydrate was heated in presence of air for 3 hr. at temperatures range from 400 ^oC and 700 ^oC. By sintering at two different temperature samples NiO400 and NiO700 were prepared at 400^oC and 700^oC. X-ray diffraction was conducted with the help of the Bruker D8 Advance X-ray diffractometer with Cu Kα radiation (0.154 nm) in the angle range 10^o–90^o. The dielectric measurement was performed with impedance analyzer model-Wayne Kerr 6500 V works in the frequency range of 20 Hz to120 MHz and in the *ac* voltage range from 10 mV to 1 V.

TABLE 1. Shows the crystallographic data using analytical analysis for NiO samples.

Intensity (%)	2θ	$Sin^2\theta$	$h^2 + k^2 + l^2$	C	(hkl)	a(Å)	$\overline{a}$(Å)
61.69	37.279	0.1022	3	0.034	(111)	4.1772	4.1775
100	43.472	0.1365	4	0.034	(200)	4.1727	
44.83	62.901	0.2722	8	0.034	(220)	4.1772	
15.68	75.416	0.3741	11	0.034	(311)	4.1772	

TABLE 2. Rietveld parameters of different NiO samples.

Compounds	a(Å)	V ($Å^3$)	Rf factor	Bregg's R-factor	R_p	R_{wp}	R_e	χ^2	*L*(nm)
NiO400	4.176	72.82	2.39	3.94	24	16.7	14.9	1.261	240
NiO700	4.172	72.64	4.04	4.51	22	15.8	13.3	1.416	350

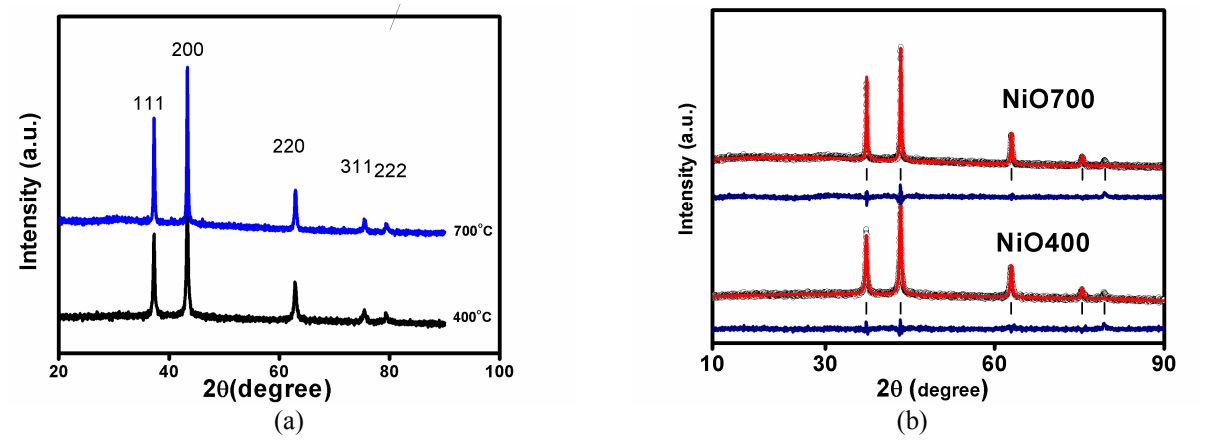

FIGURE 1. (a) X ray diffraction pattern of non stiochiometric $Ni_{1-\delta}O$. (b) Shows the Rietveld refinement fitting of XRD data.

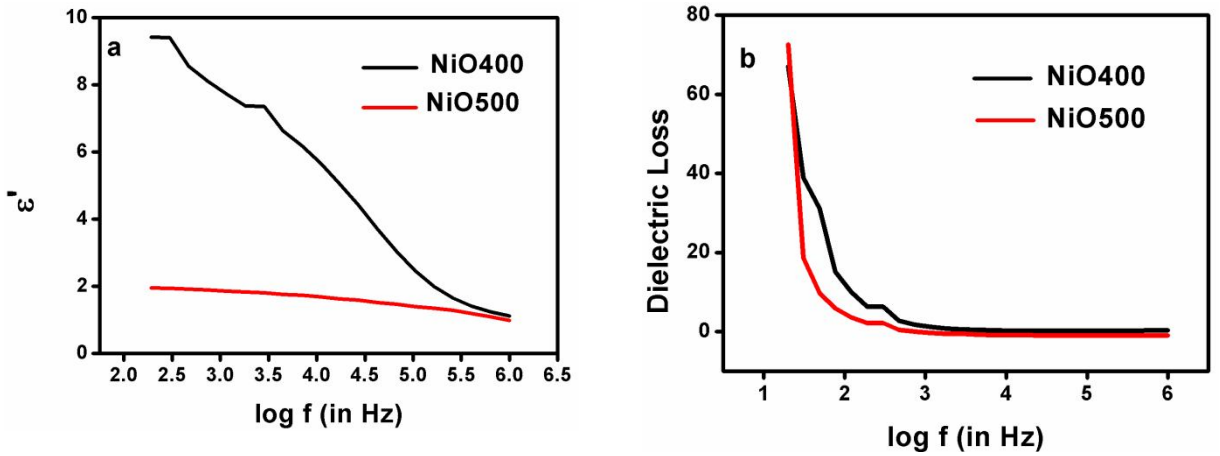

FIGURE 2. (a and b) Shows frequency dependent dielectric constant (ε`) and loss tangent (tan δ) of NiO400 and NiO700 samples recorded at room temperature.

RESULT AND DISCUSSION

XRD analysis, which is the most useful technique for identification of crystalline structure, was employed to investigate the crystallinity and purity of the solid product obtained by thermal conversion in air of the poly-nuclear coordination compounds. The XRD data of nickel oxide sample prepared at different temperature is shown in Fig. 1(a), which shows the presence of the characteristic peaks for NiO at 2θ in the range of 10^o – 90^o, in accordance with JCPDF File 78-0643. The lattice parameters were obtained from the following relationship analytically: $\sin^2\theta = C(h^2+k^2+l^2)$, where $C = \lambda^2/4a^2$. The results of the X-ray structural analysis are given in Table 1 for one of the representative samples sintered at 400 ^{o}C. Our analysis indicates good agreement between Bragg's reflection peaks obtained from analytical analysis data and the structural data of with JCPDF File 78-0643. This indicates that the NiO sample obtained by thermal conversion in air of the poly-nuclear coordination compounds, revealed the NiO with face-centered cubic phase, also known as the bunsenite structure (lattice constant *a* of cubic unit cell, 0.4177 nm). For others samples, there was also no appreciable deviation in structural data within the limit of accuracy of analytical method. No other additional peaks corresponding to other phases were emerged, suggested NiO phase is stable.

Further, the mean crystallite size of the NiO sample can be calculated using Sherrer formula: $L = k\lambda/\beta\cos(\theta)$, where L is the crystallite size, k is the Sherrer constant, usually taken as 0.89, λ is the wavelength of the x-ray radiation (0.154056 nm for Cu Kα), and β is the full width at half maximum (FWHM) of diffraction peak measured at 2θ. The deduced values of crystallite size of the analyzed NiO samples are reported in Table 2, which indicates that as the sintering temperature of precursor increases the crystallite size of NiO also increases.

We have also performed Rietveld refinements for all the samples using Fullprof software. Fig. 1(b) shows the refinement profile of all the samples in which experimental data (circles), calculated pattern (continuous line) and their difference (continuous line at the bottom) are plotted; the positions of the Bragg reflections are indicated by vertical bars. The various parameters obtained from refinement data are given in Table 2. It can be concluded that the crystal parameters obtained from analytical calculation from XRD graph and fitting the curve by Rietveld refinement corroborates each other.

Figure 2(a and b) shows the dielectric constant and dielectric loss (tan δ) with log *f* response of the NiO400 and NiO700 samples at room temperature from 20 Hz to 100 kHz. In both the samples, there is a decrease in a dielectric loss with increasing frequency. From the figure 2(a and b), it can be seen that in the case of NiO400, the dielectric constant have a higher value as compared to NiO700. For NiO400, a hump like a trend is observed in dielectric loss, which signifies the presence of relaxation in the sample. The nature of dielectric permittivity for free dipoles oscillating in an alternating field may be described as: at very low frequencies dipoles follow the field and we have $\varepsilon' = \varepsilon_s$ (value of the dielectric constant at quasistatic fields). As the frequency increases dipoles lag behind the field and $\varepsilon' = \varepsilon_\infty$ (high frequency value of ε′) [9]. Qualitatively this behavior has been observed in Fig. 2 a. The dielectric constant at low frequency is rather high and found to decrease with the increase in frequency. It is found that dielectric constant decrease with the increase in frequency. These results suggest that with the increase in frequency, the accumulation of charges also increases [13]. These accumulated charges would overcome the potential barrier at grain boundaries, which would infer that these accumulated charges are becoming mobile charge carriers. In general relaxation process of a dielectric material is described by Debye relaxation theory [14]. When frequency is low at room temperature, the electric dipoles freeze through the relaxation process. Hence there would be decay in polarization with respect to applied electric field, which is demonstrated by the decrease in dielectric constant with frequency. In general, there are two effects involved in determining the relaxation process of the material, the rate of polarization formed and the frequency of applied electric field [15]. The rate of polarization formed is quick at higher temperature and hence the relaxation process occurs at higher frequency. Fig. 2(b) shows the dependence of dielectric loss as a function of frequency. The exponential increase in tan δ with the increase in frequency depicts the increase in conductivity. At low frequency, loss factor increases which indicate the contribution of the DC conductivity which may be due to the presence of free charge carriers. Above the free charge carrier activities, the characteristic hump was observed in the tangent loss spectrum. Hence the, peaks are associated with a relaxation process.

CONCLUSIONS

Finally, nickel oxide of various stoichiometry were prepared by using a simple and inexpensive thermal decomposition technique at different sintering temperatures. The XRD studies show that all the nickel oxide samples

were crystallize in cubic phase. The dielectric constant and loss show decreasing trend because of excess oxygen and thermal activated relaxation process.

ACKNOWLEDGMENTS

Financial support from the UGC-DAE CSR, Indore under Collaborative Research Scheme is gratefully acknowledged.

REFERENCES

1. C. N. R. Rao, Annu. Rev. Phys. Chem**. 40,** 291 (1989)
2. O. Bidault, M. Maglione, M. Actis and M. Kchikech, Phys. Re. B **52,** 4191 (1995).
3. M.P. Browne, J.Electrochem.Sci. **11,** 6636 (2016).
4. M. Pinarbasi, J. Appl. Phys.**87,** 5714 (2000)
5. J. Bandara and H. Weerasinghe, Solar Energy Mat. Solar Cells **85**, 385 (2005).
6. I. Hotovy, J. Huran, S. Hascik and V. Rehacek, Sensors and Actuators B **57,** 147 (2007).
7. C. M. Lampert, Solar Energy Mater.**11**, 27 (1984).
8. H. Liu, W. Zheng, X. Yan and B. Feng, J. Alloys Compd. **462,** 356 (2008).
9. T. Badapanda, V. Senthil, S.K. Rout, L.S. Cavalcante, A.Z. Simões, T.P. Sinha, S.Panigrahi, M.M. De Jesus, E. Longo and J.A. Varela, Curr. Appl. Phys. **11**, 1282 (2011).
10. T. G. Gray, J. Phys. Chem. **60**, 201 (1956).
11. Y.Iida and S.Ozaki, J. Am. Ceram.Soc. **42,** 219 (1959).
12. Paras Dubey and Netram Kaurav, J. Phys.: Conf. Ser **836,** 012040 (2016)
13. V. Biju and M.A. Khadar, J. Mater. Sci. **38**, 4055 (2003).
14. L.A.K. Dominik and R.K. MacCrone, Phys. Rev. **163**, 756 (1967).
15. Y. Lin, L. Jiang, R. Zhao and C.-W. Nan, Phys. Rev. B **72**, 014103(2005).